

Roll convection of binary fluid mixtures in porous media

R. UMLA, M. AUGUSTIN, B. HUKÉ
AND M. LÜCKE

Institut für Theoretische Physik, Universität des Saarlandes, Postfach 151150, D-66041
Saarbrücken, Germany

(Received ?? and in revised form ??)

We investigate theoretically the nonlinear state of ideal straight rolls in the Rayleigh–Bénard system of a fluid layer heated from below with a porous medium using a Galerkin method. Applying the Oberbeck–Boussinesq approximation, binary mixtures with positive separation ratio are studied and compared to one-component fluids. Our results for the structural properties of roll convection resemble qualitatively the situation in the Rayleigh–Bénard system without porous medium except for the fact that the streamlines of binary mixtures are deformed in the so-called Soret regime. The deformation of the streamlines is explained by means of the Darcy equation which is used to describe the transport of momentum. In addition to the properties of the rolls, their stability against arbitrary infinitesimal perturbations is investigated. We compute stability balloons for the pure fluid case as well as for a wide parameter range of Lewis numbers and separation ratios which are typical for binary gas and fluid mixtures. The stability regions of rolls are found to be restricted by a crossroll, a zigzag and a new type of oscillatory instability mechanism, which can be related to the crossroll mechanism.

1. Introduction

The Rayleigh–Bénard system is one of the classical setups and possibly the most popular one to study pattern formation and hydrodynamic instabilities under well-controlled conditions. The system consists of a fluid layer bounded by two plates and is heated from below. If the temperature difference between the plates exceeds a critical value, the fluid leaves its static state and thermal convection sets in. Under appropriate conditions, the fluid flow forms a regular pattern, for example a state of ideal straight rolls (ISR), also called Bénard rolls or steady overtuning convection (SOC).

Over the last decades, the roll convection and in particular the instability mechanisms, which tend to limit the stability region of the ideal roll state, have been investigated in detail experimentally (see Busse & Whitehead (1971) and Croquette & Williams (1989)) as well as theoretically (see Busse & Clever (1979); Schlüter *et al.* (1965); Clever & Busse (1990); Bolton *et al.* (1986); Bolton & Busse (1985)). One main result of this research is that the region of rolls, which are stable against infinitesimal perturbations, is restricted by certain instability mechanisms, for instance the zigzag, the skewed varicose, the Eckhaus and the crossroll mechanism. This remains also valid if the fluid between both the plates saturates a porous medium, a case applying to many natural and industrial processes (see Vafai (2005) or Nield & Bejan (2006) for an overview). For a porous medium, Juárez & Busse (1995) investigated theoretically the stability of rolls

against two-dimensional perturbations and found the Eckhaus and an oscillatory instability mechanism. Straus (1974) did the same but allowed for three-dimensional perturbations and found a zigzag as well as a crossroll mechanism. These investigations were complemented by the experimental observation of roll convection in porous media by Shattuck *et al.* (1997) and Howle *et al.* (1997).

The aforementioned research was carried out for a one-component, i.e., a pure fluid. However, numerous applications are known where the fluid has to be treated as a binary mixture consisting of two different fluids (see for example Platten 2006). Especially, if the binary mixture shows a non-vanishing Soret effect, i.e., if concentration currents are driven by temperature gradients, the dynamics of the system are expected to change due to a coupling of the temperature field into the concentration field. For the classical Rayleigh–Bénard system without porous medium, there has been a large body of work dealing with binary mixtures under the influence of the Soret effect (Eaton *et al.* (1991); Barten *et al.* (1995); Huke & Lücke (2002); Gal *et al.* (1985); Dominguez-Lerma *et al.* (1995); Barten *et al.* (1989); Schöpf & Zimmermann (1993); Knobloch & Moore (1988); Cross & Kim (1988); Kolodner *et al.* (1986); Fütterer & Lücke (2002); Touiri *et al.* (1996); Ahlers & Rehberg (1986); Walden *et al.* (1985)). In particular, the roll convection and the corresponding stability mechanisms are well known (see Huke *et al.* (2000)). For the system with porous medium, however, the standard of knowledge is much less developed, although there has been some work concerning the stability of the ground state and mono-cellular flow by Charrier-Mojtabi *et al.* (2007), Elhajjar *et al.* (2008) and Sovran *et al.* (2001).

With this paper, we aim at extending the knowledge about flow patterns of binary mixtures in porous media by analysing the structural properties as well as the stability of the Bénard rolls. In doing this, we restrict ourselves to a positive Soret coupling in which the Soret effect destabilizes the ground state. The paper is organized as follows: In Sec. II we will briefly explain the basic equations of the system, the Galerkin method that we have used for numerical computations, the ground state and its stability. In Sec. III we discuss the properties of roll convection by investigating the structure of the fields, the advective heat transport and the mixing. Sec. IV contains the main results of our paper. Here, we represent the stability boundaries of the Bénard rolls for a pure fluid as well as for binary mixtures and compare the former ones to the known results. In Sec. V we conclude with a summary of our results.

2. Foundations

2.1. System and basic equations

We consider a horizontal layer of a porous medium filled with a pure fluid or a binary mixture in a homogeneous gravitational field, $\mathbf{g} = -g\mathbf{e}_z$. The layer has thickness d and a vertical temperature gradient is imposed by fixing the temperature

$$T = T_0 \pm \frac{\Delta T}{2} \quad \text{at} \quad z = \mp \frac{d}{2}, \quad (2.1)$$

which can be realized in experiments by using highly conducting plates. T_0 is the mean temperature of the layer and we assume $\Delta T > 0$, i.e., the lower plate has a higher temperature than the upper one. Moreover, we consider the plates to be infinitely extended, rigid and impermeable. The porous medium is treated as isotropic and homogeneous. Furthermore, we assume local thermal equilibrium between the fluid and the porous medium such that there is no heat transfer between both phases.

Convection is characterized by the fields of temperature T , the Darcy velocity \mathbf{v} (also

called seepage velocity), mass concentration C of the lighter component, total mass density $\rho = \rho_1 + \rho_2$ and pressure P . Applying the Oberbeck-Boussinesq approximation, we assume the dynamic viscosity, the thermal expansion coefficients and the heat capacities to be constant and equal to their values at the spatial averages T_0 , C_0 , P_0 of the thermodynamic variables. Moreover we neglect effects like radiation or the generating of heat due to friction between the fluid and the porous medium. For binary mixtures, the Soret effect can play an important role. We incorporate this effect in our model, which describes the generation of concentration currents due to temperature variations. Then, the balance equations for our system read according to Nield & Bejan (2006):

$$\nabla \cdot \mathbf{v} = 0 \quad (2.2a)$$

$$c_a \rho_0 \partial_t \mathbf{v} = -\nabla P - \frac{\eta}{K} \mathbf{v} + \rho_0 [1 + \beta_T T + \beta_C C] g \mathbf{e}_z \quad (2.2b)$$

$$C_{\text{tot}} \partial_t T + C_f (\mathbf{v} \cdot \nabla) T = \lambda_{\text{tot}} \nabla^2 T \quad (2.2c)$$

$$\phi \partial_t C + (\mathbf{v} \cdot \nabla) C = D_{\text{tot}} \nabla^2 C + D_{\text{tot}} \frac{\kappa T}{T_0} \nabla^2 T, \quad (2.2d)$$

Here, ρ_0 is the mean density of the fluid, η the dynamic viscosity, β_T (β_C) the thermal (solutal) expansion coefficient of the fluid and K the permeability of the porous medium. C_* denotes the heat capacity per unit volume according to its subscript f , s or tot of the fluid, the solid matrix or of the total medium (fluid and solid matrix). The heat capacities per unit volume can be connected via the porosity ϕ of the porous medium, by the relation $C_{\text{tot}} = \phi C_f + (1 - \phi) C_s$. The same holds true for the thermal conductivities λ_f , λ_s and λ_{tot} . D_{tot} is the concentration diffusivity of the total medium and is equal to ϕD whereas D is the concentration diffusivity of the fluid. The correction factor c_a emerges in front of $\partial_t \mathbf{u}$ to bring the Darcy equation (2.2b) in agreement with experimental results (see Nield & Bejan (2006)). Since the porous medium is assumed to be isotropic and homogeneous, c_a is a scalar.

In the basic equations (2.2) we scale lengths by d , time by the vertical diffusion time $\frac{d^2 C_{\text{tot}}}{\lambda_{\text{tot}}}$, temperature by $\frac{\lambda_{\text{tot}} \eta}{C_f K d \beta_T g \rho_0}$, concentration by $\frac{\lambda_{\text{tot}} \eta}{C_f K d \beta_C g \rho_0}$ and pressure by $\frac{\lambda_{\text{tot}} \eta}{C_f K}$. Moreover, we introduce the reduced deviations of the velocity $\mathbf{u} = (u, v, w)$, temperature θ , concentration c and pressure field p from the conductive state thus obtaining the following set of balance equations:

$$\nabla \cdot \mathbf{u} = 0 \quad (2.3a)$$

$$\gamma_a \partial_t \mathbf{u} = -\nabla p - \mathbf{u} + (\theta + c) \mathbf{e}_z \quad (2.3b)$$

$$\partial_t \theta + (\mathbf{u} \cdot \nabla) \theta = R w + \nabla^2 \theta \quad (2.3c)$$

$$\phi^* \partial_t c + (\mathbf{u} \cdot \nabla) c = R \psi w + L (\nabla^2 c - \psi \nabla^2 \theta). \quad (2.3d)$$

The normalized porosity $\phi^* = \phi C_f / C_{\text{tot}}$ as well as the correction factor $\gamma_a = \frac{K \lambda_{\text{tot}} \eta}{d^2 C_{\text{tot}} \rho_0} c_a$ are scalars for an isotropic and homogeneous porous medium. ϕ^* can have values in the interval $[0, 1]$ whereas γ_a is very small for usual porous materials (Nield & Bejan (2006)). Because of the smallness of γ_a , the time-derivative term in the momentum equation is often neglected (see for example Sovran *et al.* (2001) and Elhajjar *et al.* (2008)). However, we retain this term since it is - according to Vadasz & Olek (1999) or Vadasz & Olek (2000) - essential for certain stability analyses. Note that ϕ^* also appears only in front of a time derivative. Therefore, the correction factor and the normalized porosity can play a role for time-dependent phenomena only.

Via the concentration diffusivity D_{tot} , the Lewis number L is defined by

$$L = \frac{D_{\text{tot}}\phi C_f}{\lambda_{\text{tot}}}, \quad (2.4)$$

and therefore compares the time scales of concentration and heat diffusion. Note that the Lewis number as defined here is the inverse of the Lewis number Le as defined by Nield & Bejan (2006). The Rayleigh–Darcy number is given by

$$R = \frac{\rho_0 g \beta_T K C_f d}{\lambda_{\text{tot}} \eta} \Delta T \quad (2.5)$$

and measures the thermal driving. The separation ratio

$$\psi = -\frac{\beta_C}{\beta_T T_0} k_T \quad (2.6)$$

is proportional to the thermodiffusion ratio k_T thus incorporating the Soret effect which emerges via $-L\psi\nabla^2\theta$ and the term $R\psi w$ in the concentration balance equation (2.3d). In this paper, we cover mainly separation ratios from 0 to 0.5, which are typical for alcohol-water mixtures at high alcohol concentration (30-80%) and many gas mixtures, like Ne-CO₂, He-Xe, H₂-Xe and Ne-Ar (see Liu & Ahlers (1997)). That means in particular that we restrict ourselves to a positive Soret coupling ($\psi > 0$), where the lighter component of the mixture is driven into the direction of higher temperature.

In the momentum equation (2.3b), which is deduced from Darcy’s law, advective transport and diffusion of momentum are neglected. Instead, we take into account the relaxation term $-\mathbf{u}$ describing the friction between the fluid and the porous matrix, which dominates the aforementioned mechanisms at low Reynolds numbers ($Re = O(1)$). Thereby, to define the Reynolds number of a flow through a porous medium, the average radius of the pores is chosen as the characteristic length scale.

If no pressure gradient is applied to the system, there will be no mean flow. This can be deduced as follows: We decompose the velocity field

$$\mathbf{u}(x, z, t) = \hat{\mathbf{u}}(x, z, t) + U(z, t) \mathbf{e}_x \quad (2.7)$$

into a mean flow term $U(z, t) \mathbf{e}_x = \langle \mathbf{u}(x, z, t) \rangle_x$ and a part without mean flow $\hat{\mathbf{u}}(x, z, t) = \mathbf{u}(x, z, t) - U(z, t) \mathbf{e}_x$, where $\langle \hat{\mathbf{u}}(x, z, t) \rangle_x = 0$. Here, $\langle \dots \rangle_x$ denotes the lateral average in x -direction. To obtain an equation for $U(z, t)$ we take the lateral average of the x -component of the Darcy equation 2.2(a). This yields

$$\gamma_a \partial_t U(z, t) = -U(z, t). \quad (2.8)$$

Therefore, any mean flow will decay exponentially with a decay constant of $1/\gamma_a$. So we can suppose that there is no mean flow at all.

Since the fluid is assumed to be incompressible, we can write the velocity field \mathbf{u} as

$$\mathbf{u} = \nabla \times \nabla \times \begin{pmatrix} 0 \\ 0 \\ \Phi \end{pmatrix} + \nabla \times \begin{pmatrix} 0 \\ 0 \\ \Psi \end{pmatrix}, \quad (2.9)$$

which automatically fulfills the mass balance (2.3a). To derive equations for the potentials Φ and Ψ , one can apply the curl to the momentum balance equation (2.3b) once or twice, respectively and take into account only the third component of the obtained equations. Besides, this eliminates the pressure term. Moreover, the boundary conditions for the velocity field, $w = 0$ at $z = \pm \frac{1}{2}$, resulting from the rigidity of the plates, are transformed into $\Phi = 0$ at $z = \pm \frac{1}{2}$. To obtain this boundary condition for the Φ -field, we have assumed

that there is no external pressure gradient that causes a meanflow, and thus there is no meanflow in the system at all. At the impermeable plates, the vertical concentration current vanishes, i.e., $\partial_z(c - \psi\theta) = 0$ for $\pm\frac{1}{2}$. To avoid this coupling of the fields in the boundary conditions, we introduce in a next step the field

$$\zeta = c - \psi\theta. \quad (2.10)$$

The corresponding balance equation for ζ can directly be derived by combining the equations (2.3c) and (2.3d). Altogether, the new balance equations read

$$\gamma_a \partial_t \Delta_{xy} \Psi = -\Delta_{xy} \Psi \quad (2.11a)$$

$$\gamma_a \partial_t \nabla^2 \Delta_{xy} \Phi = -\nabla^2 \Delta_{xy} \Phi - \Delta_{xy}(\theta + c) \quad (2.11b)$$

$$\partial_t \theta + (\mathbf{u} \cdot \nabla) \theta = R w + \nabla^2 \theta \quad (2.11c)$$

$$\phi^* \partial_t \zeta + (\mathbf{u} \cdot \nabla) \zeta + (1 - \phi^*) (\mathbf{u} \cdot \nabla) \theta = (\phi^* - 1) R \psi \Delta_{xy} \Phi + L \nabla^2 \zeta - \phi^* \psi \nabla^2 \theta \quad (2.11d)$$

with $\Delta_{xy} := \partial_x^2 + \partial_y^2$ and the boundary conditions

$$0 = \Phi = \theta = \partial_z \zeta \quad \text{at } z = \pm\frac{1}{2}. \quad (2.12)$$

Since there is no meanflow in the system, and equation (2.11a) is a pure diffusion equation, the Ψ field will decay over time to $\Psi \equiv 0$ for any initial condition. Because we do not intend to investigate transients, we can fix $\Psi \equiv 0$ so that the equation (2.11a) becomes irrelevant in what follows.

2.2. Numerical method

To obtain roll solutions, we used the Galerkin method with the following ansatz for the fields $X = \Phi, \theta, \zeta$:

$$X(x, z) = \sum_m^{N_m} \sum_n^{N_n} X_{mn} \cos(mkx) f_n(z). \quad (2.13)$$

Since rolls are even in x with an appropriate choice of the origin, we expand using cosines in the lateral direction. The $f_n(z)$ are an orthogonal set of trigonometrical functions that fulfill the boundary conditions at the plates. We choose:

$$\text{for } \Phi, \theta : f_n(z) = \begin{cases} \sqrt{2} \cos(n\pi z) & \text{if } n = 1, 3, 5, \dots \\ \sqrt{2} \sin(n\pi z) & \text{if } n = 2, 4, 6, \dots \end{cases} \quad (2.14)$$

$$\text{for } \zeta : f_n(z) = \begin{cases} \sqrt{2} \sin(n\pi z) & \text{if } n = 1, 3, 5, \dots \\ \sqrt{2} \cos(n\pi z) & \text{if } n = 2, 4, 6, \dots \\ 1, & \text{if } n = 0. \end{cases} \quad (2.15)$$

The lateral index m starts from 0 for the θ and the ζ -field and from 1 for the Φ -field. All θ - and ζ -modes with $n + m > N$ and all Φ -modes with $n + m > N/2$ are neglected, where we choose $N = 24$ if not otherwise specified. The fact that our truncation keeps less modes in Φ than in θ and ζ is motivated by the work of Hollinger & Lücke (1998).

In addition to their symmetry in x -direction, rolls fulfil the so-called mirror-glide symmetry (see Veronis (1966)), i.e.,

$$X(x, z) = -X\left(x + \frac{\pi}{k}, -z\right). \quad (2.16)$$

As a consequence we can set one half of the modes to zero. Then, we insert the ansatz into the basic equations and project onto the ansatz functions which yields a coupled system of nonlinear algebraic equations. To solve this system, we used a Newton-Raphson algorithm.

In addition, we will test the stability of rolls against arbitrary infinitesimal disturbances. The ansatz for the perturbations reads as follows:

$$\delta X(x, y, z, t) = \sum_{m=-N_m}^{N_m} \sum_{n=-N_n}^{N_n} \delta X_{mn} e^{st+i[(d-mk)x+by]} f_n(z), \quad (2.17)$$

where $f_n(z)$, N_m and N_n agree with the definitions above. To determine the growth behaviour of such a perturbation, we add it to the known solution and insert into the basic equations. Then, we linearize the equations around the roll fixed point and project onto the ansatz functions which yields an eigenvalue problem. After transforming the corresponding eigenvalue matrix into Hessenberg form, the eigenvalues are computed using the QR algorithm for Hessenberg matrices of Press *et al.* (2002). If the eigenvalue problem yields only eigenvalues s with negative real part for every b and d , the rolls are proven to be stable. That way, one has to check all wavenumbers b in y -direction, i.e. $b \geq 0$. However, because of the periodicity of the roll patterns in the x -direction and their mirror-glide symmetry, it suffices to test only perturbations with $d \in [0, k/2)$. Another simplification due to the mirror-glide symmetry of the underlying pattern is that the perturbations can be divided into two subclasses, say, into G -perturbations (\bar{G} -perturbations) that are symmetric (antisymmetric) under the mirror glide operation $(x, z) \rightarrow -(x + \frac{\pi}{k}, -z)$ if the factor $e^{idx+iby}$ is set to 1. By this separation, the eigenvalue problem can be reduced to computing the eigenvalues of two matrices that have only half of the size (for further details see Huke *et al.* (2000)). Since calculating the eigenvalues of a matrix is an $O(N^3)$ -process, this lowers the computation time by about a factor 4. In the special case $d = 0$, the perturbations can be separated further into symmetric and antisymmetric perturbations under the operation $x \rightarrow -x$.

2.3. Ground state and linear Stability Analysis

The linear stability problem for binary mixtures of the system under consideration has already been investigated by Sovran *et al.* (2001), Charrier-Mojtabi *et al.* (2007) and Elhajjar *et al.* (2008). Having used an analytical method and a Galerkin expansion, we obtain results in good agreement with the former. In the following, we are going to review the most important facts concerning the conductive state as a preparation and introduction for the subsequent nonlinear analysis.

In the ground state, the fluid rests and heat is transported only by diffusion. The temperature difference ΔT between the plates imposes a linear temperature profile as follows:

$$T_{\text{cond}}(z) = T_0 - \frac{\Delta T}{d} z. \quad (2.18)$$

Due to the Soret effect, this temperature gradient generates a linear concentration profile of the form:

$$C_{\text{cond}}(z) = C_0 + \frac{k_T \Delta T}{T_0 d} z. \quad (2.19)$$

The pressure distribution in the conductive state is given by

$$p_{\text{cond}}(z) = p_0 + \rho g \left[\beta_T \left(T_0 - \frac{\Delta T}{d} z \right) + \beta_C \left(C_0 - \frac{k_T \Delta T}{2dT_0} z \right) \right] z, \quad (2.20)$$

which can be calculated from the concentration and temperature field via the momentum equation (2.3b). If there is a positive Soret coupling as investigated here, the lighter component of the binary fluid is driven to the lower plate. This increases the density difference between the plates and therefore destabilizes the ground state.

The destabilizing effect is illustrated in Figure 1 where the critical Rayleigh–Darcy number R_c as well as the corresponding critical wavenumber k_c is plotted against the separation ratio ψ for several L . For the pure fluid ($\psi = 0$), the ground state loses its stability above $R_c^0 = 4\pi^2 \approx 39.48$ against stationary perturbations of a lateral wavenumber $k_c^0 = \pi$. By contrast, the ground state of binary mixtures becomes already unstable for a thermal driving weaker than R_c^0 and the critical Rayleigh–Darcy number decreases with stronger Soret effect, i.e., growing ψ . In particular, if the concentration gradients are slowly diffused away, i.e., for small Lewis numbers, the destabilization is especially strong. The corresponding critical perturbations remain stationary but their wavelength k_c goes to zero for large ψ . For example at $L = 0.5$, one finds $k_c = 0$ for about $\psi \geq 1.759$ which is close to the theoretical value $\psi \geq \frac{1}{\frac{40}{51L} - 1} = 1.7586$ obtained by Sovran *et al.* (2001). In experiments, the critical wavelength will then be as large as the finite size of the convection cell allows.

3. Properties of the roll convection

3.1. Structure of the fields

To understand roll convection of a binary mixture from a qualitative point of view, one can study the temperature and concentration distribution as well as the flow field. In what follows, we give such a qualitative description by Figure 2, in which the streamlines, the concentration and temperature field along with the lateral profiles of the fields at midheight $z = 0$ are shown for several values of thermal driving. Since the behaviour remains in principle the same over a wide range of wavenumbers, we fix the wavenumber to $k = k_c^0 = \pi$. The chosen parameters, $L = 0.01$, $\psi = 0.3$, can be realized easily in experiments with alcohol–water mixtures. In this case, the critical Rayleigh–Darcy number R_c is reduced to about 0.39. The left column in Figure 2 displays the fields over one periodicity interval in x -direction for $R = 10$. This value lies in the so-called Soret regime where convection is dominated by the Soret effect. The temperature field deviates only marginally from its linear profile in the ground state, i.e., advective heat transport is weak. In contrast, the concentration field is already strongly modulated and forms plume-like structures since the slow concentration diffusion ($L \ll 1$) allows for a perturbation of the linear profile already for weak advection. The anharmonicity of the concentration field becomes obvious by looking at the lower part of Figure 2, where the lateral profile of the concentration field is plotted versus x at midheight, $z = 0$. The velocity field, represented by its z -component at midheight, is also anharmonic and the streamlines that illustrate the roll-like flow are deformed.

The middle column of Figure 2 refers to $R = 50$. This value lies in the so-called Rayleigh regime where convection would set in also without an operating Soret effect. Here, a stronger modulation of the temperature field can be seen due to an increased advective heat transport. Nevertheless, the temperature field is almost harmonic as seen from the horizontal variation of T at midheight. The concentration field shows the characteristic boundary layer behaviour: The binary fluid is well mixed in the bulk whereas pronounced concentration gradients exist at the plates and the roll boundaries. The better mixing is caused by the larger velocity of the fluid. The corresponding streamlines reflect the roll-like flow and are almost harmonic indicating that the anharmonic behaviour of the

velocity for $R = 10$ is induced by the Soret effect. This conclusion has been strengthened when we simulated the streamlines of a pure fluid and did not find any deformation provided the thermal driving was not too strong. Note furthermore that the deformation of the streamlines in the Soret regime seems to be generic for the system with porous medium. This can be explained by the replacement of the momentum diffusion term $\nabla^2 \mathbf{u}$ (contained in the Navier–Stokes equations) by the relaxation term $-\mathbf{u}$ in our momentum balance equation (2.3b). In the clear fluid, i.e., in the system without porous medium, momentum diffusion tends to smooth the spatial anharmonicity of the velocity field caused by the very anharmonic concentration field. Since the relaxation term $-\mathbf{u}$ in (2.3b) does not contain spatial derivatives, it does not provide spatial smoothing and the anharmonicity of the concentration field is imposed via the buoyancy term onto the velocity field. Taking into account that the buoyancy at $R = 50$ is caused rather by the almost harmonic temperature field than by the concentration field, it becomes clear why the streamlines are barely deformed.

When nonlinear effects are amplified further by increasing the heating rate, plume-like structures appear also in the temperature field and the concentration boundary layers become thinner. We can see this in the right column of Figure 2, where R has reached a value of 100. The streamlines are now deformed again, this time because the temperature field has become anharmonic by the intensive thermal driving.

3.2. Nusselt and mixing numbers

To describe the advective heat transport due to roll convection quantitatively, we make use of the Nusselt number Nu . The Nusselt number is given by

$$\text{Nu} := \frac{\langle j_{\text{tot},z} \rangle}{\langle j_{\text{cond},z} \rangle} \quad (3.1)$$

where $j_{\text{tot},z}$ denotes the total vertical heat current density and $j_{\text{cond},z}$ the vertical heat current density in the conductive state. $\langle \cdot \rangle$ denotes the lateral average. The Nusselt number at the plates can be computed from the modes obtained by our Galerkin method with truncation index N as follows:

$$\text{Nu} = 1 - \frac{2\sqrt{2}\pi}{R} \sum_{n=1}^N (-1)^n n \theta_{02n}. \quad (3.2)$$

Note that the Nusselt number does not actually depend on the z -position in a stationary state of convection as the rolls are.

In Figure 3 we compare Nusselt numbers of the pure fluid, which we have found to be in good agreement with the results from Juárez & Busse (1995), to Nusselt numbers of binary mixtures. In the ground state, Nu is equal to 1, since heat is transported only by diffusion. After the roll convection has started, i.e., R has exceeded R_c , the Nusselt number and simultaneously the advective heat transport increases monotonically with R . For a given Rayleigh–Darcy number, Nu is always larger for binary mixtures with $\psi > 0$ than for the pure fluid, as the Soret effect causes a concentration gradient giving rise to a more pronounced buoyancy and thus a stronger convection. For the same reason, the Nusselt number grows when the Soret effect becomes stronger, i.e., when ψ is increased. In the Rayleigh region, one might expect the binary mixture to behave similar to a pure fluid, as the advective mixing is strong. Indeed, the Nusselt number of a binary mixture with small L approaches the one of the pure fluid. However, when L becomes larger, i.e., when concentration diffusion is fast, the advective mixing does not succeed to mix away the concentration gradients. Then, the differences in Nu to the pure fluid case remain more significant. We have also found these tendencies for wavenumbers that differ from

the wavenumber $k = \pi$ chosen in Figure 3, albeit convection becomes weaker and Nu decreases if the wavenumber gets too large or too small.

The mixing of a binary fluid can be described by the so-called mixing number M , which is defined by the normalized variance of the concentration field:

$$M = \frac{\sqrt{\langle C^2 \rangle - \langle C \rangle^2}}{\sqrt{\langle C_{\text{cond}}^2 \rangle - \langle C_{\text{cond}} \rangle^2}}. \quad (3.3)$$

C_{cond} denotes the concentration field in the conductive state and $\langle \cdot \rangle$ the spatial average. From $M = 1$, which is the value of the mixing number in the ground state by definition, it decreases when roll convection sets in and the components of the binary fluid are mixed. According to Figure 4, the mixing number decreases only slightly in the Rayleigh regime when the thermal driving gets stronger. In other words, one cannot mix the fluid components perfectly by increasing R . The reason is that the fluid is already well mixed in the Rayleigh regime except for the fluid layers near to the plates and at the roll boundaries, whose thickness depends barely on R . Instead, the boundary layer behaviour in the Rayleigh region depends mainly on the Lewis number of the mixture such that the mixing number is reduced when L is lowered. The latter facts are also valid in the clear fluid case and can be explained using concentration boundary layer theory in analogy to Hollinger (1996). A larger separation ratio improves the mixing mainly in the Soret regime whereas the influence of ψ in the Rayleigh regime is rather weak.

4. Stability of the rolls

4.1. Stability boundaries for the pure fluid

Using the Galerkin method from section 2.2 with $N = 24$, we have tested the roll structure against infinitesimal perturbations of arbitrary wavenumber. For the pure fluid, similar stability analyses have been carried out by Juárez & Busse (1995) and Straus (1974). In agreement with their results, we find that only two instability mechanisms, the zigzag and the crossroll mechanism, limit the region of stable rolls. The corresponding stability boundaries in the (R, k) -parameter space are shown in Figure 5. Below, we review briefly the important instability mechanisms and compare our results to those of Straus and Juárez. If not otherwise specified, the instabilities are related to a real eigenvalue, i.e., the corresponding stability boundary does not depend on ϕ^* or γ_a .

4.1.1. Zigzag instability

The zigzag (ZZ) boundary, denoted by the dash-dotted line in Figure 5, restricts the region of stable rolls on the small- k side; if the rolls are zigzag-unstable, a new set of rolls with a larger wavenumber begins to grow. The ZZ perturbations belong to the subclass of G -perturbations that are odd in x -direction. They have the same periodicity in x -direction as the existing pattern. Consequently, we find the ZZ instability for $d = 0$. It is sufficient to check the stability only for a single point on the b -axis near $b = 0$ in order to determine whether a roll state is ZZ-stable or not (for further details see Bolton *et al.* (1986)).

Compared to the ZZ boundary calculated by Straus, ours is much more restrictive. At $R = 55$ for example, rolls should be unstable for $k < 3.046$ according to our computations whereas Straus states the same for $k < 2.5$ using an analytical criterion.

4.1.2. Crossroll instability

According to Figure 5, the region of stable rolls is mainly restricted by the crossroll (CR) boundary given by the solid line. Thus, rolls with either too large or too small

wavenumbers are destabilized by the CR instability, which causes the growth of rolls perpendicular to the existing pattern. Above $R \approx 342 =: R_h^0$, the CR mechanism destabilizes the rolls independent of their wavenumber. The CR perturbations are even in x -direction and belong to the subclass of \overline{G} -perturbations. They have the same periodicity in the x -direction as the original rolls so that we find the CR instability for $d = 0$. By contrast, the parameter b , which represents the wavenumber of the CR perturbation perpendicular to the roll pattern, cannot be fixed to test whether rolls are CR-stable. Instead, to decide this, one has to find the value b_{max} where the most critical eigenvalue reaches its maximum by applying an interpolation procedure. In Figure 5, the value of b_{max} on the CR boundary is plotted as function of k , whereby the upper section of $b_{max}(k)$ belongs to the part of the CR boundary at higher R . Near the onset, b_{max} is close to k_c^0 . For larger R , b_{max} is generally larger since the whole stability region shifts to larger k .

The above mentioned value $R_h^0 \approx 342$ differs from the one obtained by Straus who states $R_h^0 \approx 380$. Furthermore, our CR boundary is again more restrictive on the small- k side: According to our calculations, rolls with a wavenumber $k < 2.28$ are CR-unstable whereas Straus finds CR-stable rolls with $k \approx 1.8$. However, these disagreements decrease when we lower our truncation parameter N and thus we conclude that our results are more precise than those obtained by Straus.

4.1.3. Eckhaus instability

The Eckhaus (EC) boundary, denoted by the dotted line in Figure 5, lies below the CR boundary for all wavenumbers, i.e., the EC perturbations can only grow where the rolls are already CR-unstable. The EC instability tends to establish rolls with a better wavenumber in the direction of the wavevector of the original roll state. The corresponding perturbations are even in x -direction and fall into the subclass of G -perturbations. As purely two-dimensional perturbations, they are found at $b = 0$. Conveniently, the question of EC stability can be answered by investigating a single point on the d -axis near $d = 0$ (see Juárez & Busse (1995)). Our result for the EC boundary agrees well with the one obtained by Juárez.

Since we have found no other instability mechanisms inside the ZZ- and CR-stable region, we conclude that within this stability region rolls are stable against arbitrary infinitesimal perturbations. In particular, rolls are stable at the critical point (R_c^0, k_c^0) . Note that the stability region discussed above is similar to the stability balloon of the clear fluid at large Prandtl numbers for No-slip boundary conditions computed by Busse & Clever (1979) as well as for Free-slip boundary conditions computed by Bolton & Busse (1985): In each of the three cases, the region of stable rolls is restricted by the ZZ boundary on the small- k side and otherwise by the CR boundary. The similarity of the stability balloons can be understood using a heuristic argument. The influence of the advective term and the time derivative term in the Navier–Stokes equation becomes small for large Prandtl numbers so that it resembles the Darcy equation for small γ_a except of the fact that the relaxation term in (2.3b) is replaced by a diffusion term.

4.2. Stability boundaries for binary mixtures

Figure 6 shows the EC, ZZ and CR boundary for binary mixtures below $R = 80$. We cover a range of separation ratios ranging from 0.01 to 0.4 and Lewis numbers from 0.1 to 1. Again, the stability boundaries are found to be in qualitative agreement with those of the clear fluid for large Prandtl numbers, computed by Huke *et al.* (2000): In the Rayleigh regime, the ZZ boundary $R_{ZZ}(k)$ lies close to the corresponding line of the pure fluid and shifts slightly to smaller k if ψ is increased. At the transition between the Rayleigh and the Soret region, $R_{ZZ}(k)$ bends towards small k (see for instance $L = 0.5$ and $\psi = 0.05$).

By decreasing R further on, the ZZ boundary terminates with a finite slope at the critical point (R_c, k_c) . The EC boundary $R_{EC}(k)$ is also connected to the onset, from where it opens up parabolically. For small L , the EC boundary deviates from the parabolic shape and shows a vase-like form at the transition from the Soret to the Rayleigh regime (see for example $L = 0.1$ and $\psi = 0.05$). In the Rayleigh region, $R_{EC}(k)$ as well as the ZZ boundary lie close to the corresponding line of the pure fluid. The most important fact regarding the EC boundary is that it lies beyond the CR boundary for all investigated (L, ψ) -combinations. Therefore, the EC instability occurs only where the rolls are already unstable to CR perturbations. For $L = 1$, which is a typical value for gas mixtures, the CR boundary is still connected to the critical point (R_c, k_c) . However, for smaller L and sufficiently large ψ the CR boundary detaches from the neutral curve. In this case rolls are no longer a stable form of convection at the onset. We observed square convection at the onset instead as it has also been seen in the clear fluid case by Dominguez-Lerma *et al.* (1995), Huke *et al.* (2000), Müller & Lücke (1988) and Moses & Steinberg (1991).

The whole (R, k) -regions of stable rolls are shown in Figure 7. Inside the closed curve defined by the CR boundary rolls are stable to CR perturbations. For large ψ and small L , the CR boundary shifts to larger wavenumbers and is the only stability boundary limiting the region of stable rolls (see $L = 0.1$ and $\psi = 0.4$). Otherwise, the CR-stable region is intersected by the ZZ boundary on the small- k side. For the presented parameter range, we have detected no other instability mechanisms inside the ZZ- and CR-stable region. Thus, the regime of stable rolls is limited exclusively by the ZZ and the CR boundary in analogy to the pure fluid.

The CR boundary defines the lowest Rayleigh–Darcy number R_l as well as the highest one R_h , for which rolls are stable. As seen from the dotted lines in the first row of Figure 8, R_h decreases when the separation ratio grows. By contrast, R_l , denoted by the solid lines in the first row of Figure 8, grows with increasing ψ as soon as the CR boundary becomes detached from the neutral curve. Altogether, the region of stable rolls shrinks with increasing Soret effect. Note that this is also valid where the CR boundary is not detached from the ground state and R_l is given by R_c , which is depicted by the dashed lines in the first row of Figure 8. Considering the curvature of $R_l(\psi)$ and $R_h(\psi)$ it seems that CR-stable rolls cannot exist for too large separation ratios. This conjecture is also supported by further numerical tests: We have found no CR-stable rolls for the parameters $L = 0.1$ and $\psi = 0.5$ on an equidistant grid in the (R, k) -plane with $\Delta R = 5$ and $\Delta k = 0.05$.

The wavenumber k_l (k_h) of the marginally stable rolls at R_l (R_h) is shown in the second row of Figure 8 as solid (dotted) lines. Note that k_l is equal to k_c when the CR boundary is connected to the neutral curve. By increasing ψ , k_h decreases whereas k_l grows when the CR boundary is detached from the neutral curve. The same trend holds for the wavenumber b_l (b_h) in y -direction of the most critical CR perturbation at (R_l, k_l) ((R_h, k_h)), which are displayed as solid (dotted) lines in the third row of Figure 8. While b_l lies near to k_l and b_h is similar to k_h , they are not exactly the same.

4.3. Stability boundaries for binary mixtures with small L

Up to now we did not cover the case of Lewis numbers as small as $L = 0.01$, which is a typical value for many kinds of liquids. Two stability balloons for binary mixtures with $L = 0.01$ are shown in Fig. 9 for separation ratios of $\psi = 0.01$ (left) and $\psi = 0.1$ (right). We first investigate the case of $\psi = 0.01$. The EC boundary does not change qualitatively, neither does the ZZ boundary. For small Rayleigh-Darcy numbers we also find a CR boundary being similar to the ones we have seen before. More interesting is the appearance of a new stability boundary, which is marked in Fig. 9 by a dash-

double-dotted line in the upper part of the balloons. It precedes the CR boundary for sufficiently large values of R . The corresponding eigenvalue reaches its maximum for $d = 0$ but for different b in each point of the stability boundary. Moreover, the corresponding perturbations fall in the subclass of \overline{G} -perturbations and are even in x -direction. As we can see, this new boundary is rather similar to the CR boundary, and it ends on the latter at smaller values of R . However, the difference between the CR boundary and the new boundary is that the corresponding eigenvalue of the latter is complex, i.e. the boundary corresponds to an oscillatory perturbation.

In order to clarify the relationship between this new boundary and the CR boundary, we have a look at the eigenvalues. Figure 10 shows the real parts of the two eigenvalues with the greatest real parts vs. b for different wavenumbers k at parameters $L = 0.01$, $\psi = 0.01$, $R = 290$, $\phi^* = 1$ and $\phi^* = 0.7$, respectively. Let us follow these curves from small to large b . If we consider $k = 6.07$, there is only one curve because the two relevant eigenvalues form a pair of complex conjugated eigenvalues for all shown b . For the other examined values of k , this pair splits up into two real eigenvalues, which merge again at larger b . If $\phi^* = 1$, both eigenvalues become positive as a complex pair. So the corresponding stability boundary is oscillatory. But if $\phi^* = 0.7$, the eigenvalues split up while they are still negative and only the larger one of the two now real eigenvalues becomes positive. So, in this case, the corresponding stability boundary is stationary. We see that both, the new boundary and the CR boundary, are generated by the same eigenvalue and should thus be understood as one boundary. We call the oscillatory part oscillatory crossroll (OCR) boundary. It appears at small L and sufficiently large R depending on ψ .

As a time dependent phenomenon, the OCR boundary also depends on ϕ^* and γ_a . The influence of ϕ^* can already be seen from the eigenvalues we have discussed before. With decreasing ϕ^* the OCR boundary moves towards the CR boundary and the points at which the boundary changes from stationary to oscillatory behaviour move to larger R . For sufficiently small ϕ^* the boundary is stationary for all values of R . To study the influence of γ_a , we varied this parameter between 10^{-4} and 10^{-9} . The curves we obtained differ only slightly. For example, at fixed R , the relative differences of the wavenumbers changes less than 0.1% when γ_a changes from 10^{-4} to 10^{-9} . Moreover, the relative differences between the values for γ_a and $\gamma_a/10$ tend to 0, i.e. the curves converge. The minor influence of γ_a can be explained by comparing the time scales of velocity, temperature and concentration. In nondimensional units, the diffusion time of the temperature field is one while the diffusion time scale of the concentration field is given by the Lewis number which in this case is $L = 0.01$. Compared to these the time scale of the velocity field given by γ_a is at least a hundred times larger than the other time scales for all investigated values. As a result we can say that the time derivative in the velocity equation (2.3b) may be neglected for our stability analysis as long as the time scale given by γ_a is distinctly smaller than all other time scales in the system. We did not investigate the case that γ_a and L have the same order of magnitude which is rather unusual. Therefore, we cannot exclude that there may be relevant changes in the stability boundaries in such a case.

Further research turned out to be difficult. For example at $\psi = 0.1$ (right plot in Fig. 9) the boundaries did not converge by enhancing the number of modes in our model up to $N = 40$, the largest model we used. The boundaries shown here can be considered as qualitatively but not quantitatively correct. Notice that the ZZ boundary is no longer connected to the ground state but bent up once more to larger R by entering the Soret regime. The critical wave number here is zero and amplitude equation models that would require the ZZ boundary to end at the critical point do not apply anymore. The CR

boundary seems not to be a closed curve any longer. For $\phi^* = 1$ we find the OCR boundary in a large R -range. Also the gap between the OCR and CR boundary becomes larger.

5. Conclusion

We studied theoretically roll convection of pure fluids and binary mixtures in the Rayleigh–Bénard system with porous medium using a Galerkin method. The Soret effect was taken into account whereas we restricted the investigations to mixtures of positive separation ratio.

The state of convection has been investigated qualitatively in terms of the streamlines as well as the structure of the temperature and concentration field and quantitatively in terms of the Nusselt number and the mixing number. Whereas the behaviour of the Nusselt and mixing number as well as the behaviour of the temperature and concentration field resembles the situation in the clear fluid case, the behaviour of the streamlines was found to be different. In the Soret regime, the streamlines were deformed since the concentration field transferred its anharmonicity via the buoyancy term into the velocity field. For the clear fluid, this deformation is smoothed by the ∇^2 -operator in the diffusion term. However, for a fluid in a porous medium, the diffusion term is replaced by a relaxation term in the momentum balance equation deduced from Darcy’s law such that the deformation persists. At the transition to the Rayleigh regime, the deformation diminishes since from there on the buoyancy force is generated rather by the harmonic temperature field than by the anharmonic concentration field.

Also, we investigated the stability of rolls against arbitrary infinitesimal perturbations. The stability region for a pure fluid was found to be restricted by the ZZ instability and the CR instability only which is in qualitative agreement with the one of Straus (1974). However, compared to Straus (1974), our stability balloon is more restrictive on the small- k side and the highest R for which rolls should be stable against infinitesimal perturbation is calculated to about 342 instead of 380 stated by Straus.

In a next step, we extended the stability analysis to binary mixtures with $\psi > 0$. For not too small Lewis numbers ($L \geq 0.1$), the ZZ and the CR instability mechanism were found again to be the only relevant mechanisms. The corresponding stability boundaries changed similarly to the clear fluid case: In the Rayleigh regime, the ZZ boundary was shifted slightly to smaller k when we increased ψ and bent towards smaller k at the transition to the Soret regime. The CR boundary was found to be detached from the neutral curve for sufficiently large ψ . Moreover, the CR stable region shrank for growing separation ratio. Thus, for example, we found no stable rolls for $\psi \geq 0.5$ and $L = 0.1$.

For small Lewis numbers such as $L = 0.01$, we observed a change in the behaviour of the CR boundary. For strong thermal driving, the critical eigenvalue corresponding to the CR boundary becomes complex. Therefore, the boundary changes to an oscillatory one. Up to now, this phenomenon has not been observed in the clear fluid system. The point at which the boundary changes from stationary to oscillatory is dependent of ψ and ϕ^* . When ϕ^* becomes small enough, the CR boundary is stationary for all values of R . Further research for larger ψ turned out to be difficult because the computed boundaries did not converge. For $\psi = 0.1$ we found that the CR boundary becomes oscillatory in a larger R -range and that the stationary CR boundary does not seem to form a closed curve any longer.

Motivated by the work of Vadasz (for example Vadasz & Olek (1999)), we retained the time derivative in the momentum balance provided with the correction factor γ_a .

Whereas, this term was essential in the stability analyses of Vadasz, we did not observe any noteworthy influence on our results as γ_a was varied in the range from 0 to 10^{-4} .

REFERENCES

- AHLERS, G. & REHBERG, I. 1986 Convection in a binary mixture heated from below. *Phys. Rev. Lett.* **56** (13), 1373–1376.
- BARTEN, W., LÜCKE, M., HORT, W. & KAMPS, M. 1989 Fully developed traveling-wave convection in binary fluid mixtures. *PRL* **63**, 376–379.
- BARTEN, W., LÜCKE, M., KAMPS, M. & SCHMITZ, R. 1995 Convection in binary fluid mixtures. i. extended traveling-wave and stationary states. *Phys. Rev. E* **51** (6), 5636–5661.
- BOLTON, E. W. & BUSSE, F. H. 1985 Stability of convection rolls in a layer with stress-free boundaries. *J. Fluid Mech.* **150**, 487–498.
- BOLTON, E. W., CLEVER, R. M. & BUSSE, F. H. 1986 Oscillatory instabilities of convection rolls at intermediate prandtl numbers. *J. Fluid Mech.* **164**, 469–485.
- BUSSE, F. H. & CLEVER, R. M. 1979 Instabilities of convection rolls in a fluid of moderate prandtl number. *JFM* **91**, 319.
- BUSSE, F. H. & WHITEHEAD, J. A. 1971 Instabilities of convection rolls in a high prandtl number fluid. *J. Fluid Mech.* **47**, 305–320.
- CHARRIER-MOJTABI, M. C., ELHAJJAR, B. & MOJTABI, A. 2007 Analytical and numerical stability analysis of solet-driven convection in a horizontal porous layer. *Physics of Fluids* **19** (12).
- CLEVER, R. M. & BUSSE, F. H. 1990 Convection at very low prandtl numbers. *Physics of Fluids* **2**, 334–339.
- CROQUETTE, V. & WILLIAMS, H. 1989 Nonlinear competition between waves on convective rolls. *Phys. Rev. A* **39**, 2765–2768.
- CROSS, M. C. & KIM, K. 1988 Linear instability and the codimension-2 region in binary fluid convection between rigid impermeable boundaries. *PRA* **37**, 3909.
- DOMINGUEZ-LERMA, M. A., AHLERS, G. & CANNELL, D. S. 1995 Rayleigh-bénard convection in binary mixtures with separation ratios near zero. *Phys. Rev. E* **52** (6), 6159–6174.
- EATON, K. D., OHLSEN, D. R., YAMAMOTO, S. Y., SURKO, C. M., BARTEN, W., LÜCKE, M., KAMPS, M. & KOLODNER, P. 1991 Concentration field in traveling-wave and stationary convection in fluid mixtures. *PRA* **43**, 7105.
- ELHAJJAR, B., CHARRIER-MOJTABI, M. C. & MOJTABI, A. 2008 Separation of a binary fluid mixture in a porous horizontal cavity. *Phys. Rev. E* **77** (2).
- FÜTTERER, C. & LÜCKE, M. 2002 Growth of binary fluid convection: Role of the concentration field. *Phys. Rev. E* **65** (3).
- GAL, P. LE, POICHEAU, A. & CROQUETTE, V. 1985 Square versus roll pattern at convective threshold. *Phys. Rev. Lett.* **54** (23), 2501–2504.
- HOLLINGER, ST. 1996 Theorie der ausgedehnten stationären und wandernden konvektion in binären fluidmischungen. PhD thesis, Universität des Saarlandes, unpublished.
- HOLLINGER, ST. & LÜCKE, M. 1998 Influence of the solet effect on convection of binary fluids. *PRE* **57**, 4238.
- HOWLE, L. E., BEHRINGER, R. P. & GEORGIADIS, J. G. 1997 Convection and flow in porous media. Part 2. Visualization by shadowgraph. *J. Fluid Mech.* **332**, 247–262.
- HUKE, B. & LÜCKE, M. 2002 Convective patterns in binary fluid mixtures with positive separation ratios. In *Thermal Nonequilibrium Phenomena in Fluid Mixtures* (ed. W. Köhler & S. Wiegand), *Lecture Notes in Physics Monographs*, vol. 584, pp. 334–354. Berlin: Springer-Verlag.
- HUKE, B., LÜCKE, M., BÜCHEL, P. & JUNG, CH. 2000 Stability boundaries of roll and square convection in binary fluid mixtures with positive separation ratio. *JFM* **408**, 121.
- JUÁREZ, M. DE LA TORRE & BUSSE, F. H. 1995 Stability of two-dimensional convection in a fluid-saturated porous medium. *J. Fluid Mech.* **292**, 305–323.
- KNOBLOCH, E. & MOORE, D. R. 1988 Linear stability of experimental solet convection. *PRA* **37**, 860–870.
- KOLODNER, P., PASSNER, A., SURKO, C. M. & WALDEN, R. W. 1986 Onset of oscillatory convection in a binary fluid mixture. *PRL* **56**, 2621–2624.
- LIU, J. & AHLERS, G. 1997 Rayleigh-bénard convection in binary-gas mixtures: Thermophysical properties and the onset of convection. *Phys. Rev. E* **55** (6), 6950–6968.

- MOSES, E. & STEINBERG, V. 1991 Stationary convection in a binary mixture. *Phys. Rev. A* **43**, 707–722.
- MÜLLER, H. W. & LÜCKE, M. 1988 Competition between roll and square convection patterns in binary mixtures. *Phys. Rev. A* **38**, 2965–2974.
- NIELD, D. A. & BEJAN, A., ed. 2006 *Convection in Porous Media*. New York: Springer-Verlag.
- PLATTEN, J. K. 2006 The soret-effect: A review of recent experimental results. *J. of Applied Mech.* **73**, 5–15.
- PRESS, K. H., TEUKOLSKY, S. A., VETTERLING, W. T. & FLANNERY, B. P., ed. 2002 *Numerical Recipes in C++*. Cambridge: Cambridge University Press.
- SCHLÜTER, A., LORTZ, D. & BUSSE, F. H. 1965 On the stability of steady finite amplitude convection. *J. Fluid Mech.* **23**, 129–144.
- SCHÖPF, W. & ZIMMERMANN, W. 1993 Convection in binary fluids: Amplitude equations, codimension-2 bifurcation, and thermal fluctuations. *PRE* **47**, 1739–1764.
- SHATTUCK, M. D., P.BEHRINGER, R., JOHNSON, G. A. & GEORGIADIS, J. G. 1997 Convection and flow in porous media. part 1. visualization by magnetic resonance imaging. *J. Fluid Mech.* **332**, 215–245.
- SOVRAN, O., CHARRIER-MOJTABI, M. C. & MOJTABI, A. 2001 Naissance de la convection thermo-solutale en couche poreuse infinie avec effet soret. *Comptes rendus de l'Académie des sciences. Série Ib, Mécanique* **329**, 287–293.
- STRAUS, J. M. 1974 Large amplitude convection in porous media. *J. Fluid Mech.* **64**, 51–63.
- TOURI, H., PLATTEN, J. K. & CHAVEPEYER, G. 1996 Effect of the separation ratio on the transition between travelling waves and steady convection in the two-component rayleigh-benard problem. *Eur. J. Mech. B* **15**, 241–257.
- VADASZ, P. & OLEK, S. 1999 Weak turbulence and chaos for low prandtl number gravity driven convection in porous media. *Transport in Porous Media* **37**, 69–91.
- VADASZ, P. & OLEK, S. 2000 Route to chaos for moderate prandtl number convection in a porous layer heated from below. *Transport in Porous Media* **41**, 211–245.
- VAFAI, K., ed. 2005 *Handbook of Porous Media*. New York: Springer-Verlag.
- VERONIS, G. 1966 Large-amplitude Bénard convection. *J. Fluid Mech.* **26**, 49–68.
- WALDEN, R. W., KOLODNER, P., PASSNER, A. & SURKO, C. M. 1985 Traveling waves and chaos in convection in binary fluid mixtures. *Phys. Rev. Lett.* **55** (5), 496–499.

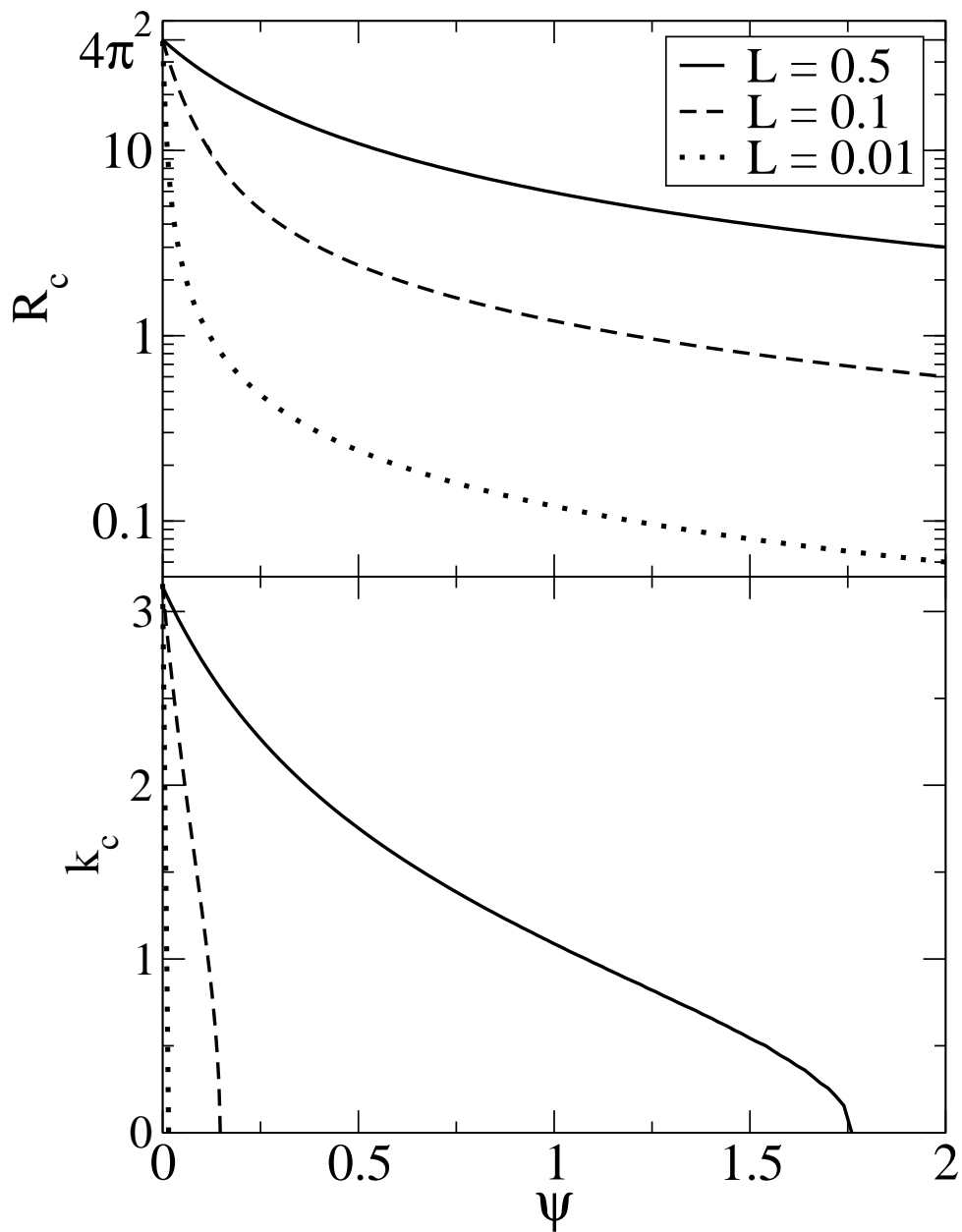


FIGURE 1. In the upper (lower) part, the critical Rayleigh–Darcy number of the ground state (corresponding critical wavenumber) is plotted against the separation ratio ψ for several L . If the thermal driving is weaker than the critical value, the conductive state is stable against arbitrary infinitesimal perturbations, otherwise at least one unstable mode exist.

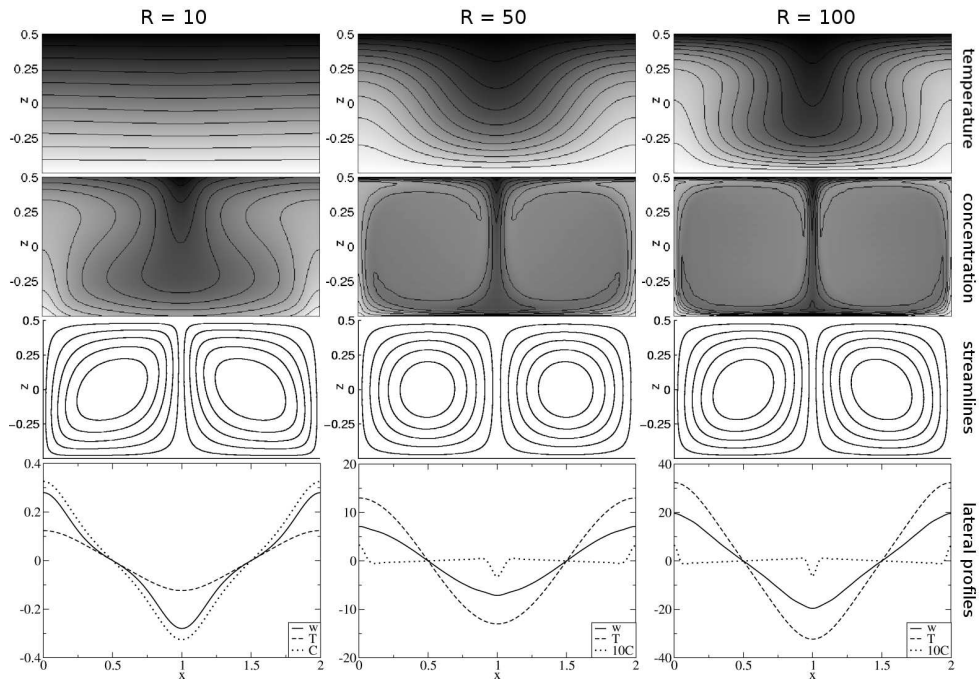


FIGURE 2. Structure of roll convection. Shown are from top to bottom the fields of temperature and concentration, the streamlines as well as the lateral profiles at midheight, $z = 0$. Parameters are $\psi = 0.3$, $L = 0.01$, $k = \pi$.

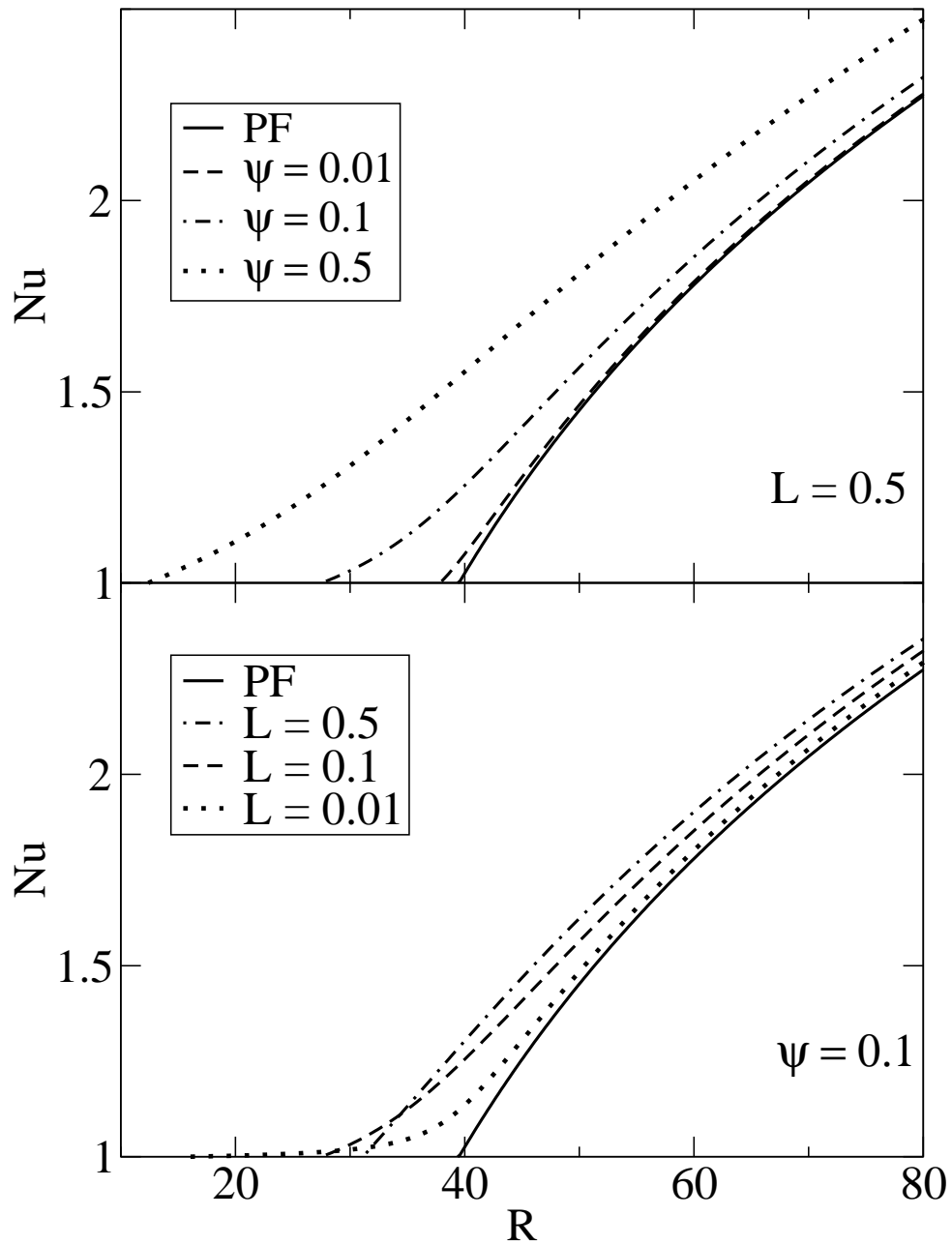


FIGURE 3. Nusselt number Nu versus Rayleigh–Darcy number R . The parameters are $L = 0.5$ in the top figure and $\psi = 0.1$ in the bottom one. In each case the wavenumber is $k = \pi$. PF denotes the pure fluid.

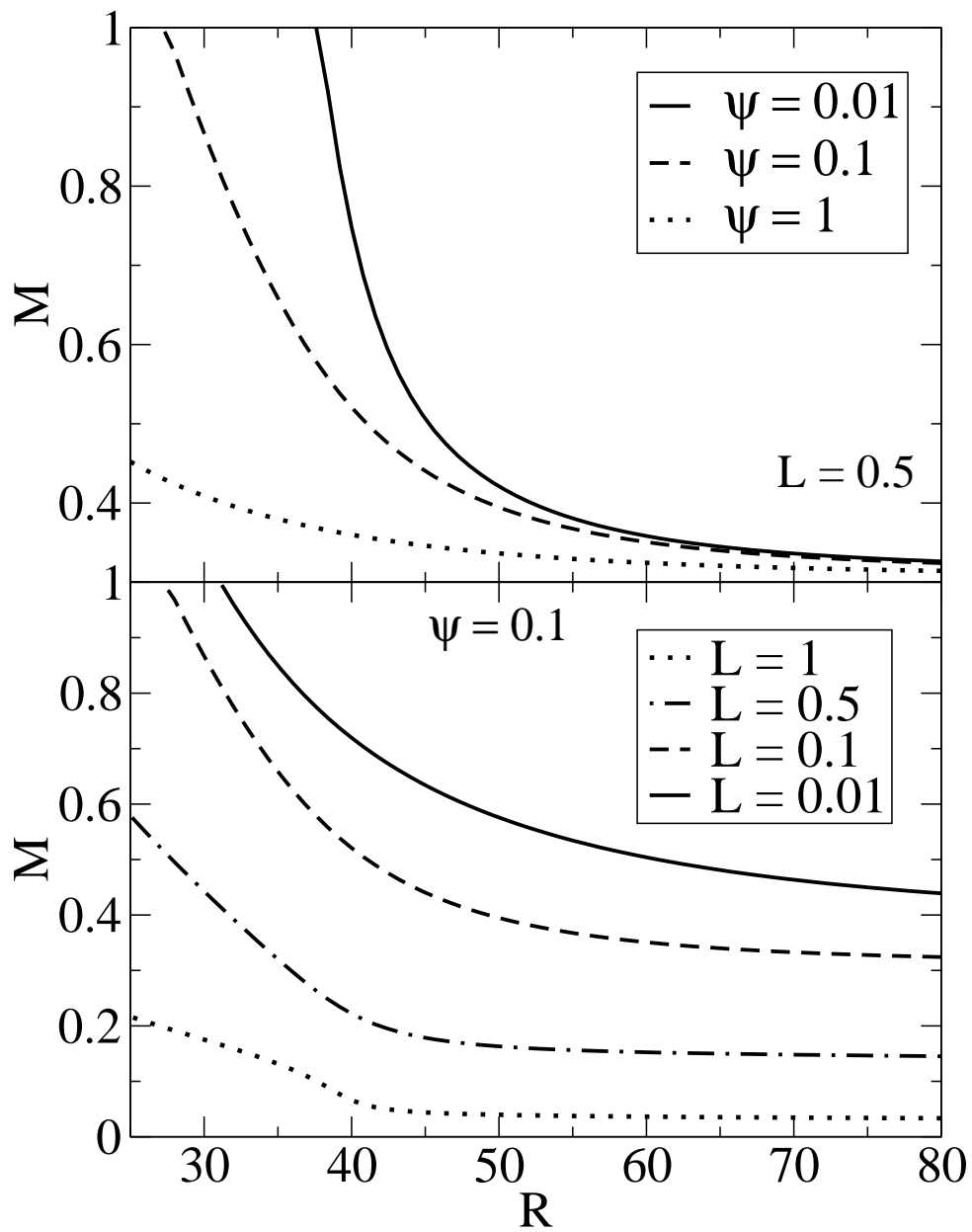


FIGURE 4. Mixing number M versus R . The parameters are $k = \pi$ and $L = 0.5$ top, $\psi = 0.1$ bottom.

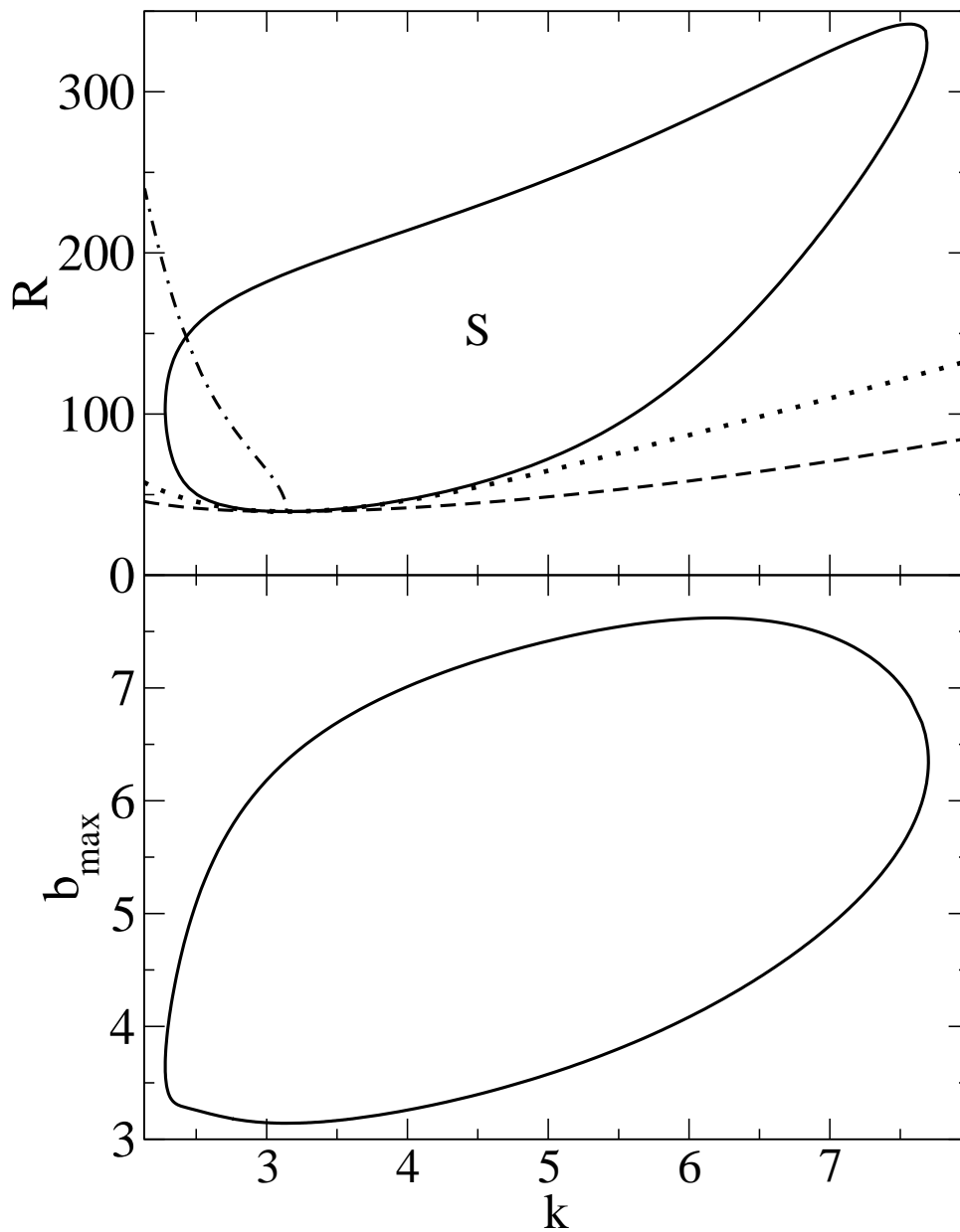


FIGURE 5. Upper part: Stability boundaries in the (k, R) -plane for the pure fluid. The Eckhaus boundary is denoted by the dotted curve, the zigzag boundary by the dash-dotted one, the crossroll boundary by the solid one and the neutral curve by the dashed one. The S marks the region of stable rolls. Lower part: b_{\max} on the crossroll boundary.

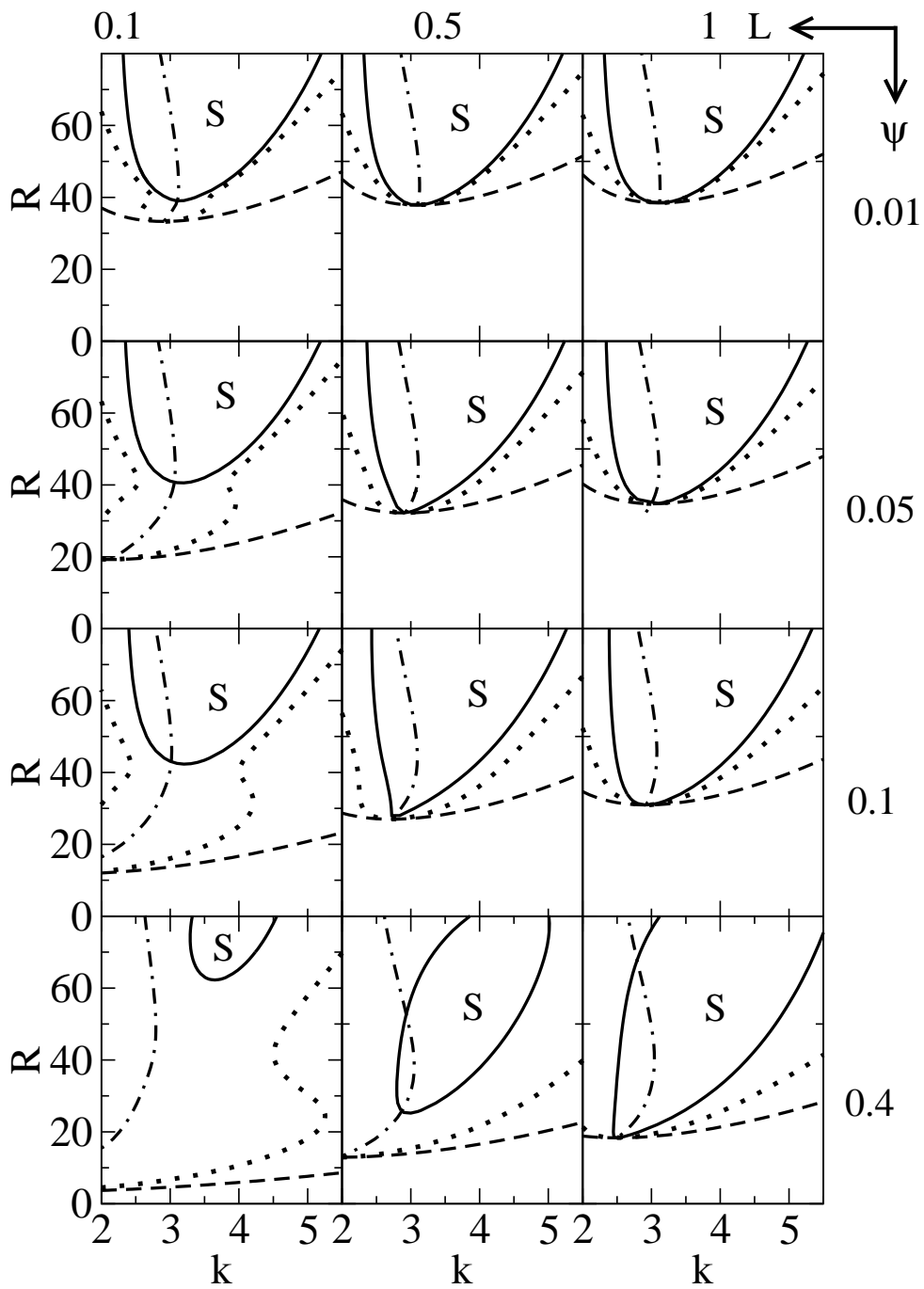


FIGURE 6. Stability boundaries in the (k, R) -plane for several combinations of L and ψ below $R = 80$. The EC boundary is denoted by the dotted curve, the ZZ boundary by the dash-dotted one, the CR boundary by the solid one and the neutral curve by the dashed one. The S marks the region of stable rolls.

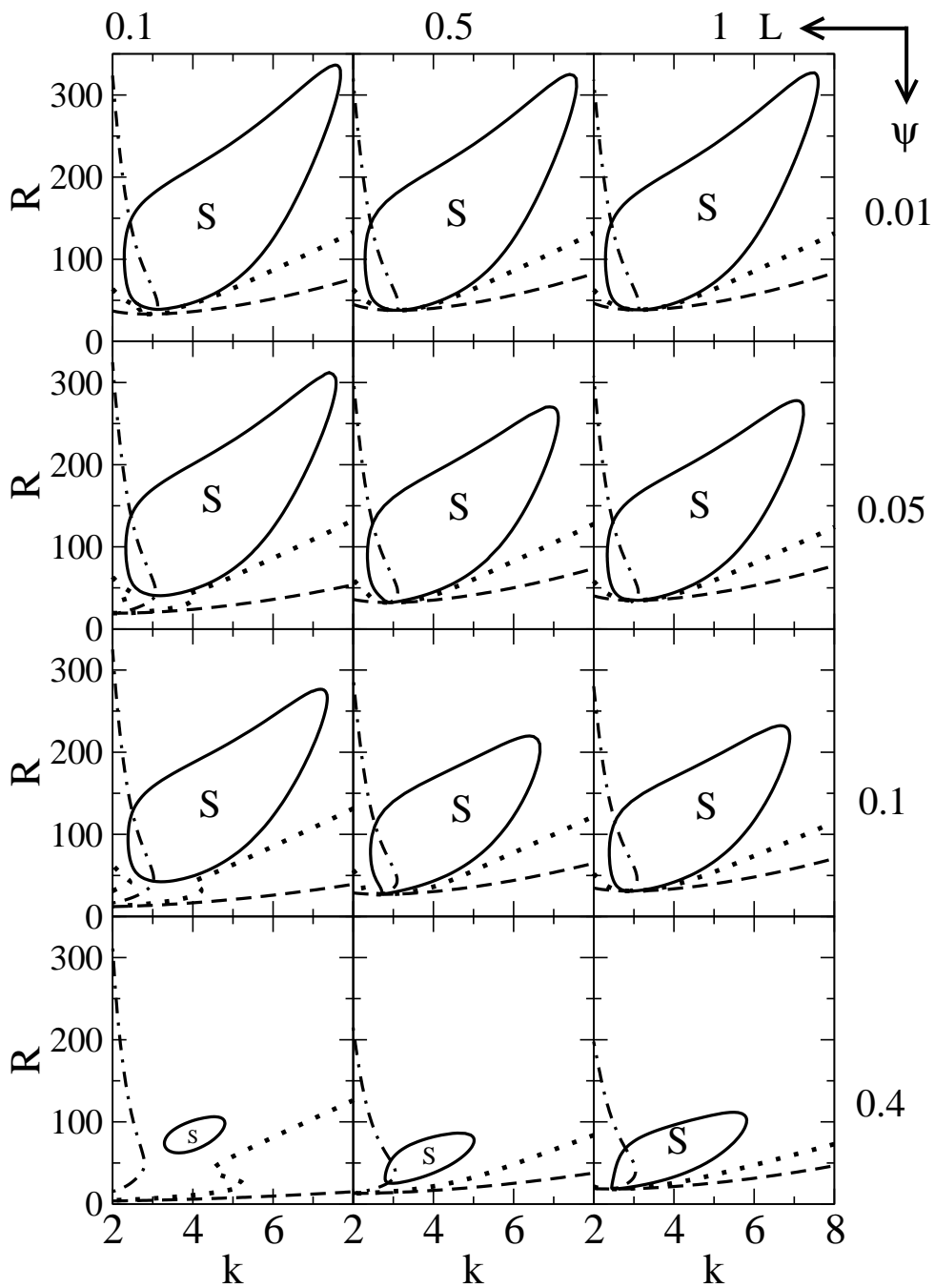


FIGURE 7. Full stability balloons in the (k, R) -plane for several combinations of L and ψ . The curve style is the same as in Figure 6.

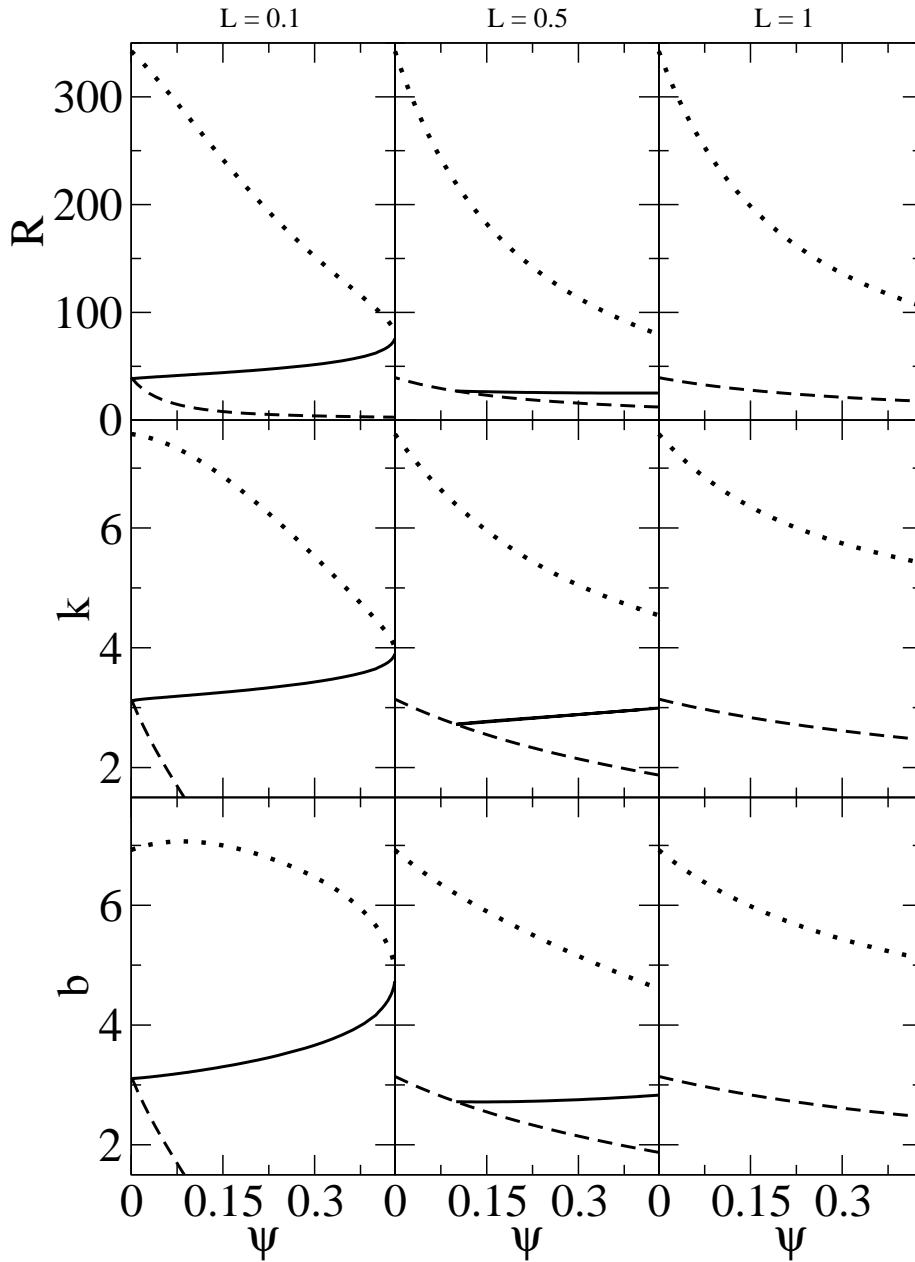


FIGURE 8. First row: For three different Lewis numbers, R_h , R_l and R_c denoted by the dotted, solid, dashed lines, respectively, are plotted versus ψ . Second row: The corresponding wavenumbers k denoted in analogy to the first row. Third row: ψ versus b_h , b_l and b_c denoted in analogy to the first row. For further details see text.

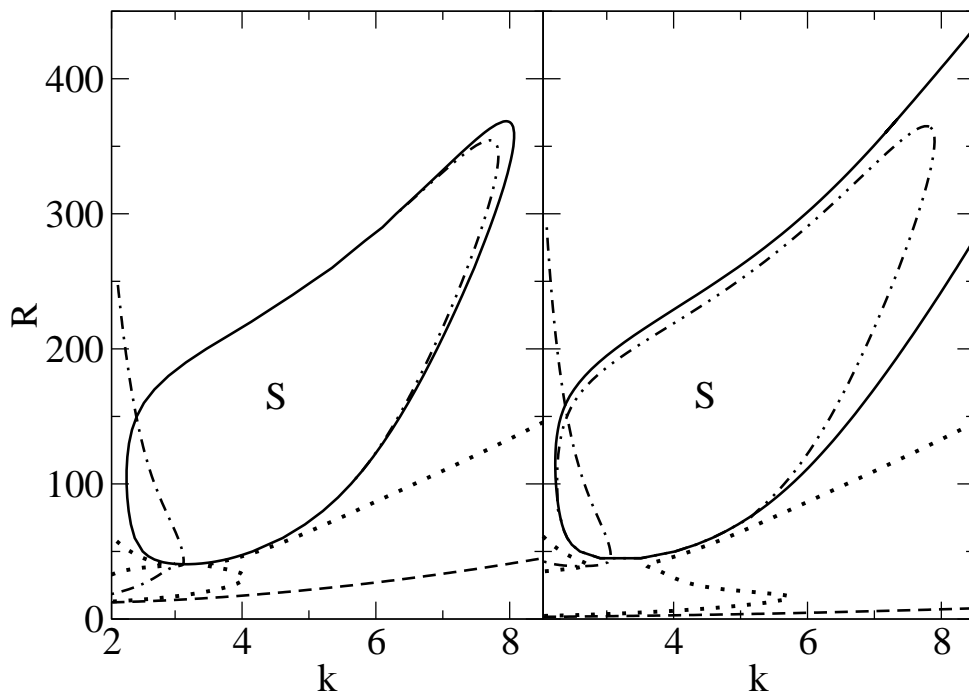


FIGURE 9. Full stability balloons in the (k, R) -plane for $L = 0.01$ and $\psi = 0.01$ (left) and $\psi = 0.1$, respectively (right). The curve style is the same as in Figure 6, except that the new OCR boundary is denoted by the dashed-double-dotted line.

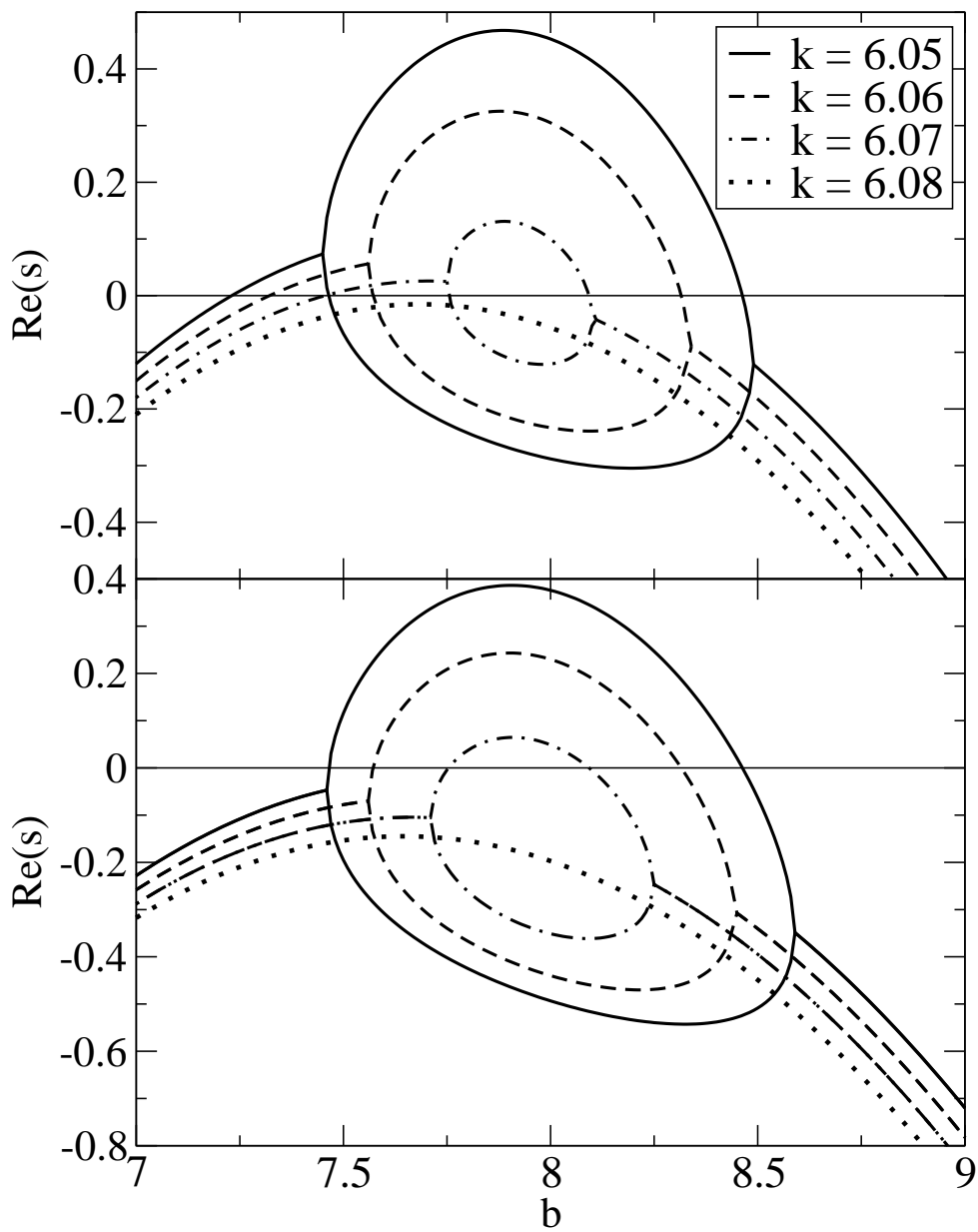


FIGURE 10. Eigenvalues of the OCR and CR boundary at $L = 0.01$, $\psi = 0.01$, $R = 290$, $\phi^* = 1$ and $\phi^* = 0.7$, respectively, for different values of the wavenumber k as indicated. Plots show the real parts of the two eigenvalues with the greatest real parts.